Space Charge Redistribution in Epoxy Mold Compounds of High-Voltage ICs at Dry and Wet Conditions: Theory and Experiment

Space Charge Redistribution in Epoxy Mold Compounds of High-Voltage ICs at the Dry and Wet Conditions: Theory and Experiment

Woojin Ahn and **Muhammad Ashraful Alam**
Department of ECE, Purdue University
West Lafayette, IN 47907 USA

Davide Cornigli and **Susanna Reggiani**
Advanced Research Center for Electronic Systems "E. De Castro" (ARCES)
Department of Electronics (DEI), University of Bologna
40136 Bologna, Italy

Dhanoop Varghese and **Srikanth Krishnan**
Texas Instruments Incorporated,
Dallas, TX 75243 USA.

ABSTRACT

Space charge profile plays an important role in defining the charge transport and breakdown field of an insulator. Non-destructive experimental techniques (e.g., PEA measurement) have recently been used to track in-situ the time-evolution of space charge profiles within complex insulators, such as epoxy mold compounds. Unfortunately, the published results are often inconsistent (both positive and negative charge build-up have been reported), and the discrepancy remains unexplained. In this paper, we (i) derive a physics-based compact analytical model of homocharge injection, (ii) explain the time- and voltage-dependent redistribution of homo- and heterocharge, (iii) investigate experimentally and explain theoretically the importance of moisture ingress regarding space charge redistribution, and finally, (iv) summarize strategies to suppress space-charge related instability in modern ICs encapsulated by epoxy mold compounds.

Index Terms — **Molding compounds, space charge, compact analytical modeling, finite element simulation, PEA measurement, DC conductivity measurement, water.**

1 INTRODUCTION

SINCE Langmuir first recognized the existence of charge injection from metallic electrodes [1], it is well-known that time-dependent space charge accumulation in insulators (e.g., Ethylene-vinyl acetate [2], polymer decoupling capacitors for high-voltage integrated circuits [3], Nitride/SiO_2/HfO_2 laminate in implanted electronics [4], epoxy mold compounds (EMCs) for modern integrated circuits (ICs), etc.) distorts the internal electric field and degrades the insulator through partial discharge, electrical tree growth, dielectric breakdown. Given the technological importance, a number of thermal, acoustic, and optical characterization methods have been invented, implemented, and validated. Among them, non-destructive characterization techniques, such as pulsed electro-acoustic (PEA) measurement, are particularly attractive due to their simplicity and robustness as well as the insights the results offer through precise tracking of the time-evolution of the space-charge in the insulator.

Manuscript received on 23 June 2021, in final form 21 October 2021,
Corresponding author: W. Ahn.

The phenomenon of space-charge injection becomes more complicated with moisture ingress in insulators exposed to harsh environmental conditions, such as in implantable electronics, undersea and overhead power lines, solar modules, and high-voltage automotive electronics. Enhanced ion transport in moisture-impregnated EMC insulators, for example, leads to electrode corrosion and destabilizes transistors presumably protected by the EMCs [4]. While the general reliability issues are well known, an extensive literature review [5-13] shows confusing and contradictory trends (see Figure 1) regarding the transient response of homocharge injection and the amount of heterocharge accumulation as a function of fillers fraction and relative humidity of the environment. The physical origin of these confusing differences has neither been explained nor modeled.

In a previous contribution [14], we investigated moisture ingress in EMC packed by polydispersed fillers to the random-close-packing (RCP) limit and proposed a compact analytical model of moisture uptake as a function of filler configuration and relative humidity. The goal of this paper is to explore, through experiment and simulation, the moisture-dependent

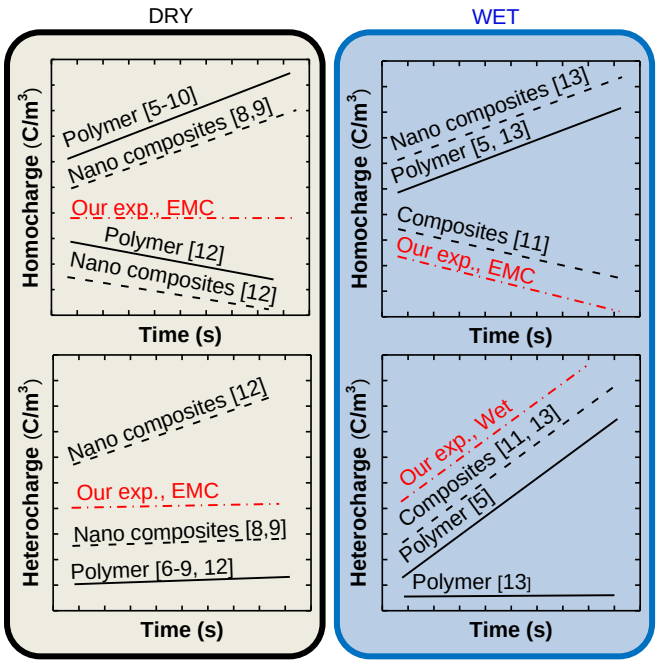

Figure 1. Diversity of results reported in the literature regarding the transient buildup of homocharge and heterocharge in dry and wet samples.

space-charge transport in composite insulators such as EMCs. In particular, we (i) perform PEA measurement and DC current measurement of commercial EMCs under dry and humid environment; (ii) investigate the impact of water on important parameters (i.e., mobility, trapping, and detrapping coefficient) based on the observations from experimental data, and numerical simulation set up; (iii) develop a compact analytical model of transient homocharge injection from the electrodes; (iv) discuss the origin of homo- and heterocharge packets, and the key characteristics of a good encapsulant for HV-ICs under humid environment. Viewed as a companion contribution to Refs. [14-17], this paper would provide a deep and nuanced understanding of the correlation between time-evolution of homo and heterocharges and the transport variables (e.g., mobility, trapping and detrapping rate) that dictate charge-buildup in polymer molding compounds with and without fillers in a dry and wet environment.

2 EXPERIMENTAL RESULTS

2.1 MATERIAL (COMPOSITES PROPERTIES, EXPERIMENTS CONDITION)

The encapsulation materials used in this study are epoxy-based conventional EMCs employed in semiconductor packaging. These encapsulant materials based on commercial-grade thermoset-based polymeric composites were provided by Texas Instruments. A detailed analysis of the filler size distribution, the interfacial properties between the filler and the epoxy, etc., are shown in Table 1 and discussed in detail in Refs. [14-17]. Specifically, the filler content was measured by thermogravimetric analysis (TGA) to determine the weight percentage (i.e., 91 wt%). In contrast, the filler volume fraction (i.e., 84%) has been calculated from the densities of the epoxy matrix and fillers by using the mean size of filler particles.

Table 1. Filler configuration and geometric information of MCs used in this work for PEA measurements.

	M73	**M90**	**M91**	**MX87** (No adhesion Promoters)
Mass $[g]$	4.88	5.54	5.72	5.66
Filler amount [%]	73 / 60 (Weight/Volume)	90 / 83 (Weight/Volume)	91 / 84 (Weight/Volume)	87 / 74 (Weight/Volume)
Filler size $[\mu m]$	~20 / ~75 (Average/Max)	~25 / ~135 (Average/Max)	~20 / ~75 (Average/Max)	~20 / ~75 (Average/Max)

Measurements have been carried out on square-shaped samples with area $A = 50\ \text{mm} \times 50\ \text{mm}$ and thickness $h = 0.75\ \text{mm}$; these samples were initially baked in a thermostatic oven at 90°C for 24h to remove any unintentionally absorbed moisture. Subsequently, a climatic chamber is used to control the humidity conditions for wet measurements.

2.2 TRANSIENT DC CURRENT MEASUREMENT

To understand the diversity of results related to a time-dependent buildup of homo and heterocharge in dry vs. wet samples (see Figure 1), we measured DC conductivity of EMCs as the sample gradually saturates with water from the dry state. The quasi-static characterization of the EMC operated at high-temperature, high voltage, under a dry environment is shown in [15]. However, an in-situ characterization in a high-humidity environment is a difficult technical challenge. Figure 2a and 2b show our newly developed and highly specialized experimental setup to measure the time evolution of the current-voltage characteristics of the EMC during moisture ingress. The high voltage cell has been specifically designed to protect the electrical connections from the humidity present in the climatic chamber, thereby avoiding electrode corrosion and preventing discharges. The system can withstand temperatures up to 150 °C. The contact area between the sample and the electrodes is hermetically sealed with two O-rings. The external area of the sample absorbs the humidity. The cell is made of aluminum, Teflon, and inox to withstand this high temperature. The pressure between sample and electrodes is controlled by three screws on the top of the cell as shown in Figure 2a, and 2b. The experiments have been carried out as follows:

1. The sample is initially dried at 90 ℃ for 24 h to desorb any residual moisture in the sample. Once the sample is dry, the transient current is measured after the application of a step-voltage with V=3kV until the steady-state is reached (about 7000s). This initial setup is important to distinguish between contact polarization vs. carrier conduction.
2. Next, the RH inside the climatic chamber is increased from 0% to 85%. Figure 2c shows the DC current measured from this step (i.e., $t = 0$ when the climatic chamber is activated). The time evolution of the current is monitored until the transient current of the moisture-infused EMC once again reaches a steady-state.
3. After the absorption stage, the RH humidity is set again to zero (i.e., desorption stage). The current is measured until it returns to its initial dry steady-state value.

Figure 2d shows that the quasi-steady-state conductivity (i.e. $\sigma(t) = I\,(t) \cdot h\,/(A \cdot V)$, based on the data in Figure 2c) increases exponentially as water saturates within the

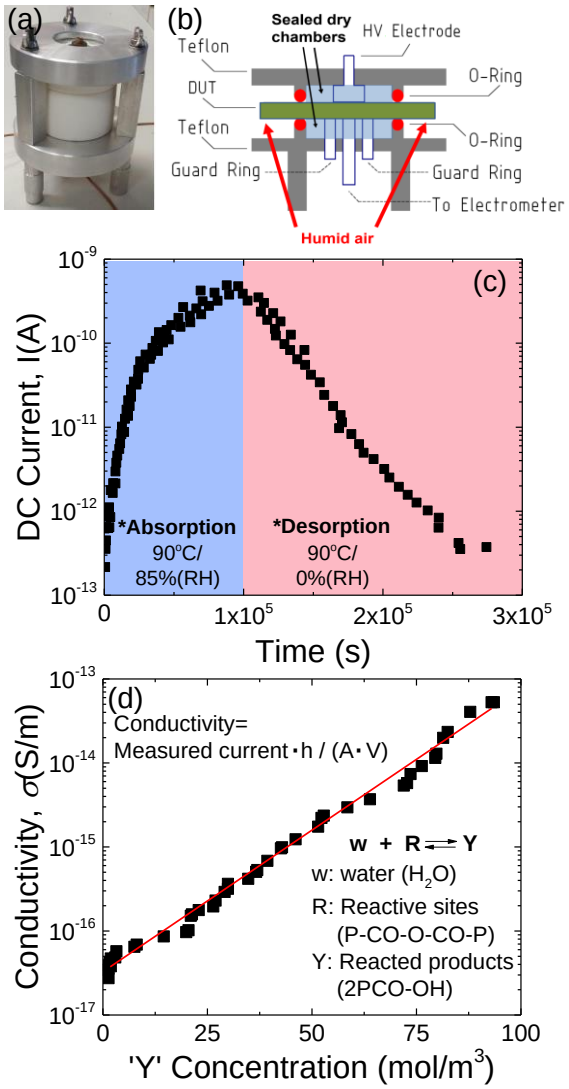

Figure 2. (a), and (b) High-voltage cell and schematic for real-time current measurements in wet conditions. (c) Transient DC current measurement results. Initially, the sample is fully dried and exposed to the humid condition. At $\mathbf{1 \times 10^5}$s, the sample is dried again. (d) Relationship between conductivity and reacted water.

encapsulant. The result is obtained as follows. Our previous work [14] has quantified the dominant impact of reacted water (Y) compared to mobile water (w) in determining the conductivity of a sample. Specifically, the reaction process (i.e. $w \rightleftarrows Y$), defines the relative contributions of mobile water concentration (w), and reacted water concentration (Y) at the anhydride groups in the polymer. Based on the DC conductivity obtained from Figure 2c and the numerical modeling of reacted water content [14, 18], we can define an empirical relationship (red line, Figure 2d) between reacted water concentration and conductivity as shown in Equation 1:

$$\sigma(t) = \sigma_0 \cdot \exp\left(\frac{Y(t)}{12.8}\right) \quad (1)$$

Here, σ_0 is the conductivity measured under dry condition, i.e. $Y(t=0) = 0$.

While the $I(t) - V$ characteristics provide the macroscopic features of MC's conductivity, and space-charge injection into the encapsulant [15-17], it does not differentiate between homo- and hetero-charge injection, nor the time-evolution of the spatial distribution of these charges. In the following section, we use the PEA profiling to obtain this information.

2.3 PEA MEASUREMENTS

The PEA analysis is performed to measure space charge distributions in MCs. An extensive literature review, including our PEA data [17], is reported in Figure 1 showing an inconsistent homo and heterocharge packet behavior. Our PEA measurements are done as follows. The time evolution of the space charge of dry (Figure 3a~3d) and wet (Figure 3e~3h) EMC samples was measured at 60 °C for 5000s (dry) 7000s (wet) in the presence of a poling field of 20 kV/mm. The moisture content of the wet samples was about 0.21% wt, i.e., close to the saturation moisture content for the EMC compound [14]. There are several important features of space charge injection related to dry and wet samples, as shown in Figure 3. For example, both types of samples appear to reach quasi-steady-state distribution relatively quickly, but we observe that the distribution evolves differently for dry and wet samples.

2.3.1. DRY CONDITION (FIGURE 3A~4D) OBSERVATIONS

1. The MCs with an adhesion promoter experience significant homocharge injection and rapid saturation to steady-state. The injected charges do not change significantly over time.
2. In MCs without adhesion promoter (i.e., MX87), the homocharge injection reduces with time, and heterocharge increases logarithmically with time. The heterocharge may have been generated by pre-existing ions with higher mobility due to the lower deep trap concentration resulted from the absence of the surface treatment given by the adhesion promoter [19].
3. Among the MCs with adhesion promoter (i.e., M73, M90, and M91), M90/M91 have higher homocharge injection compared with M73, presumably due to higher injection efficiency associated with the effective relative permittivity [20], and increasing trap concentration with increasing filler content [19].

2.3.2. WET CONDITION (FIGURE 3E~4H) OBSERVATIONS

1. Our experiments show that, except M90, all EMC samples show a time-dependent reduction in homocharge injection around the cathode. This is consistent with the results reported in [16]. This is in contrast to polymers and nanocomposites where homocharge injection is known to increase with time [5, 13] as shown in Figure 1.
2. Heterocharge injection increases logarithmically with time for all the samples, with MX87 showing the highest concentration. The heterocharge may have been generated by the dissociation of water molecules (H3O+, and OH-) [21], pre-existing ions, and charges injected from the opposite electrodes with higher mobility [21].

In the following two sections, we will discuss these characteristic features of charge injection in wet and dry samples through a phenomenological model as well as numerical simulation suitable for quantification and reliability analysis of EMC for a variety of stress conditions.

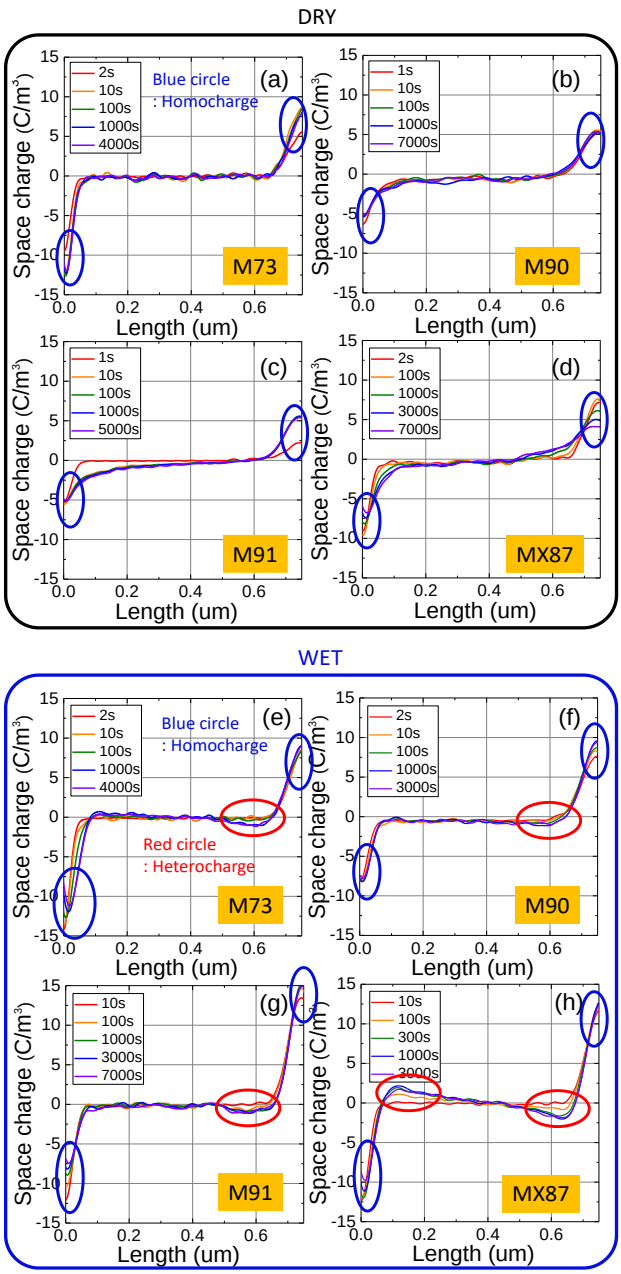

Figure 3. PEA measurements of the time-evolution of the spatial distribution of charge profiles following a step-voltage stress. **(a-d)** Dry samples and **(e-h)** wet samples. The space charge type is shown by blue, and red circles for homocharge and heterocharge, respectively.

3 NUMERICAL SIMULATION

Based on the transient DC current (Figure 2) and PEA measurement (Figure 3), here are the key differences regarding space charge injection between dry and wet EMCs.

1. DC measurement shows the current increases more than two orders of magnitude during moisture absorption. During moisture desorption, the current drops and returns to the initial level. Thus, we may conclude charge conduction directly correlates to the moisture content in the sample.
2. At the beginning of PEA measurement, the sample in the humid environment shows more homocharge injection. There is no evidence of heterocharge injection.
3. As time passes, PEA measurement of the wet sample shows a decrease of homocharge concentration close to the electrode and a simultaneous gradual increase in heterocharge at the opposite electrode.

In order to understand moisture impact on the sample's conductivity and space charge behavior, we perform finite-element method (FEM) numerical simulation based on bipolar charge transport model involving injection, transport, trapping, and recombination mechanisms. This general FEM simulation framework has been frequently used to understand charge dynamics in insulators [10]. Instead of repeating the details, we have summarized in the appendix the specific boundary conditions, the corresponding differential equations (Table A1), and the parameter values (Table A2). The need for such a self-consistent simulation has been emphasized in [16], and the corresponding steady-state ion distribution is summarized in Figure 4. The model focuses on pre-existing ions: the applied electric field is insufficient (i.e., <160MV/m) for field-ionization of encapsulant molecules [22]. For simplicity, we assume that the ionic mobility parameter implicitly encapsulates the effects of capture/emission from shallow traps. In addition to the applied voltage, sample thickness, dielectric constant (ε_r), etc., the space charge profiles are dictated by ion mobility (μ), trapping (B), and detrapping (S) coefficients as shown in Figure 4. In this paper, we have used the experimental data and the numerical parametric studies to qualitatively explain the salient features of homo and heterocharge buildup in dry vs. wet samples. Once the parameters (e.g. mobility, trapping and detrapping time-constants, position distribution of ions) are known, the models will help interpret the experimental results quantitatively.

The key to understanding the space-charge distribution is the importance of reacted water (Y) in defining the ionic mobility (i.e. conductivity) within a sample [14]. As explained in [23], the mobility increase is due to hydrolysis that generates polar and hydrophilic ions (e.g., hydronium ions leading to a formation of a liquid layer around fillers). Figure 4a shows when the sample is dry and the ion mobility is low, the charge profile is exclusivity defined by homo-charge injection, consistent with the experimental observation in Figure 3a-3d. However, following moisture ingress, the reacted water increases heterocharge (i.e., pre-existing ionic impurities) mobility and counter-charges accumulate close to the electrode, consistent with the experimental results in Figure 3e-3h.

Figures 4b and 4c show that the details of the shape of the space-charge distribution depend sensitively on trapping and detrapping parameters (B and S). For example, as B decreases, the width of the hetero-charge injection is rapidly suppressed. Similarly, increasing S is correlated to the additional heterocharge build-up at the same stress time. Comparing to the PEA measurement, it appears that S increases with moisture ingress and leads to a rapid build-up of heterocharge. On the other hand, the PEA measurement suggests that the width of the heterocharge does not depend sensitively on time, indicating B may not play a critical role in interpreting these experiments.

In summary, the build-up of homo-charge (injected from the contacts) and hetero-charge (related to pre-existing ions) depend on the applied stress, the geometry, processing details,

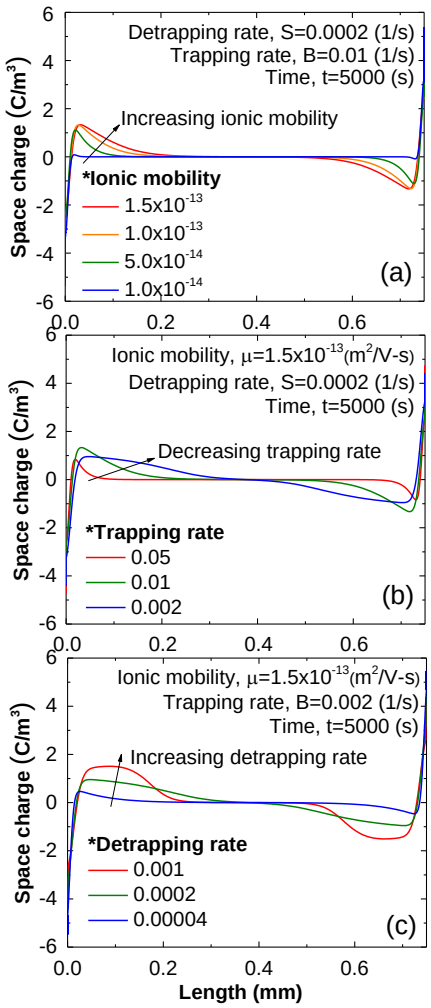

Figure 4. FEM simulation results with electrons, holes, cations, and anions. Different variables have been changed to investigate their impact of: (a) mobility, (b) trapping coefficient, (c) de-trapping coefficient.

and material parameters associated with the mold compounds, and the moisture-assisted mobility and trapping/detrapping rates of the ions within the polymer. The characteristic features of the space-charge profiles can be used to extract these parameters for reliability projections.

4 COMPACT ANALYTICAL MODEL

Intrigued by the key observations of the moisture impact on the conductivity and space charge behavior obtained experimentally and numerically, in this section, we derive a simple analytical model for the time-dependent space charge concentration at the electrode.

Ever since the establishment of non-destructive measurement techniques, several numerical studies [2] have been performed based on transport, continuity, and Poisson equations (as in Table A1) to interpret the spatial profiles obtained experimentally. Given the apparent complexity of the differential equations, the exact analytical solution is impossible. Indeed, even the approximate analytical models are too complicated [24] and do not offer significant physical insights. In this section, we will integrate the transient electric field, $E(t)$, field-dependent charge injection, and charge continuity equation to derive a simple physics-based analytical model of the space charge profile close to the electrode. Although the model is approximate (i.e., it does not provide the details that can be obtained from FEM simulation, see Figure 4), it provides important insights regarding homo and hetero-charge injection in EMCs.

4.1 TRAPPED-FREE SPACE CHARGE LIMITED CURRENT (SCLC) CASE

First, for the sake of simplicity, let us focus on the field-enhanced charge injection from the anode (or cathode) into the surrounding idealized (i.e. trap-free) encapsulant. We will consider trapping and detrapping processes later. To derive an expression for charge build-up next to the electrode, we must first solve for the time-evolution of electric-field, $E(t)$, due to injected charges into the dielectric.

A. Transient electric field on electrode: Once the voltage is applied to the sample, an initial electric field (E_0) surrounds the electrode. Many experiments have demonstrated considerable charge injection from the electrode immediately after the voltage stress. No matter what we apply for the field-dependent charge injection model, one needs to know $E(t)$ self-consistently to quantify the time-evolution of charge injection from the electrode. Based on Gauss's law, we can calculate $E(t)$ generated by a constant current density J_0, see Equation 2:

$$E(t) = E_0 - \frac{J_0 \cdot t}{\varepsilon_r \cdot \varepsilon_0} \tag{2a}$$

$$\frac{E(t)}{E_0} = 1 - \frac{t}{t_C} \quad \text{, where } \left(t_C \equiv \frac{\varepsilon_r \cdot \varepsilon_0 \cdot E_0}{J_0}\right) \tag{2b}$$

where J_0 (A/m^2), ε_r, and ε_0 (F/m) are initial charge injection flux, Faraday number, dielectric constant, and vacuum permittivity, respectively. The normalization form of Equation 2a is shown in 2b by defining a new parameter t_C.

B. Transient charge injection on electrode: In this work, we assume Schottky emission for the charge injection as shown in Equation 3:

$$\frac{J(t)}{J_0} = A_0 \cdot T^2 \cdot exp\left(\frac{-q \cdot \phi_B}{kT}\right) \cdot exp\left(\frac{q}{kT}\sqrt{\frac{q}{4\pi\varepsilon_r\varepsilon_0}} \cdot \sqrt{\frac{E(t)}{E_0}}\right) \tag{3}$$

where A_0(A/m$^2 \cdot$ K^2), k(J/K), T(K), and ϕ_B(V) are Richardson constant, Boltzmann constant, temperature, and barrier height, respectively. Once we insert Equation 2 in Equation 3, we can explain the reduction in current as the homocharge build-up screens the electrode and decreases $E(t)$.

C. Transient space charge concentration: The injected current density of Equation 3 gives the current density in the MC at the electrode. Generally, in MCs the applied voltage is large while the charge distribution and relative density gradient is small. We can thus simplify the transport equation by omitting diffusion term [24]. At the cathode, the drift term is $q\,\mu_n \cdot n_m(t) \cdot E(t)$, where μ_n and n_m are the electron mobility and the electron concentration, respectively. Equating Equation 3 and the drift term shown above, we find an expression of the charge buildup next to the electrode, namely,

$$n_m(t) = \frac{J(t)}{q \cdot \mu_n \cdot E(t)} \tag{4}$$

In principle, $J(t)$, $E(t)$, and $n_m(t)$ should be calculated self-consistently for a precise comparison with experimental data. Fortunately, the FEM simulation shows that for $t < t_C$, the

approximate formula is essentially exact, see Figure 5. When $t > t_C$, the charge injection is so small so that the inaccuracy of the approximate formula is irrelevant. By taking the time derivative of Equation 4, we can predict increase or decrease of concentration over time. In the following section, we will generalize Equation 4 and derive an expression for $n_{\mathrm{m}}(t)$ by explicitly accounting for the trapped charge.

4.2 AN ANALYTICAL MODE FOR TRAPPED SPACE CHARGE LIMITED CURRENT (SCLC)

Irregular topological structure and chemical disorder in polymer composites can be approximated as physical or chemical defects (in an otherwise idealized polymer) because they can trap mobile charges. Trapping and detrapping can distort the space charge profile significantly, leading to a modification of $E(x,t)$ within the bulk. However, the electric field at the electrode, $E(0,t)$, is not significantly perturbed by bulk defect as it depends primarily on the metal/EMC interface properties (e.g., Schottky barrier height) and ε_{r}. Thus, Equation 2 and 3 can be assumed unaltered in the trapping case as well. For the simplicity, we assume the trapping and detrapping processes involving a single trap level. The corresponding time-dependence of the mobile charge concentration $n_{\mathrm{m}}(t)$ is given by Equation 5.

$$\frac{\partial n_{\mathrm{t}}}{\partial t} = -\frac{\partial n_{\mathrm{m}}}{\partial t} = B \cdot n_{\mathrm{m}} \cdot \left(1 - \frac{n_{\mathrm{t}}}{N_{\mathrm{t}}}\right) - S \cdot n_{\mathrm{t}} \tag{5}$$

where B $(1/s)$, S $(1/s)$, and N_{t} (mol/m^3) are trapping, detrapping coefficient, and maximum trap concentration, respectively. Let us now consider two specialized cases involving fast trapping and slow trapping.

When trapping process is slow (i.e., B is small), n_{t} scales with B because we can neglect the terms: $1 - n_{\mathrm{t}}/N_{\mathrm{t}}$, and $S \cdot n_{\mathrm{t}}$. In this case, $n_{\mathrm{t}}(t)$ is given by Equation 6.

$$n_{\mathrm{t}}^{\mathrm{s}}(t) = n_{\mathrm{m}}(t) \cdot B \cdot t \tag{6}$$

When trapping process is fast, the quasi-equilibrium condition is reached immediately (i.e., Equation 5 can be set to zero, see Equation 7).

$$n_{\mathrm{t}}(t) = n_{\mathrm{m}}(t) \cdot \left(\frac{B \cdot N_{\mathrm{T}}}{S \cdot N_{\mathrm{T}} + B \cdot n_m(t)}\right) \tag{7}$$

To summarize, the total space charge concentration in a polymer at the proximity of the electrode is given by the sum of mobile charge (Equation 4) and trapped charges (Equation 6 or Equation 7 depending on trapping process speed).

To validate the analytical model, we perform FEM simulations by solving the transport, continuity, and Poisson equations simultaneously. As shown in Figure 5, the analytical model and FEM simulation produce comparable results. As time approaches t_C, there is a ~10% deviation due to the self-consistency issue between the electric field and injected flux. However, considering the typical value of t_{C} is greater than 10^4 s, it is sufficient to apply our compact model to analyze the experimental data measured with PEA.

5 DISCUSSION OF THE KEY EXPERIMENTAL/SIMULATION RESULTS

The appearance of heterocharge shown in Figure 3e-3h in wet EMC samples has variously been explained by two different

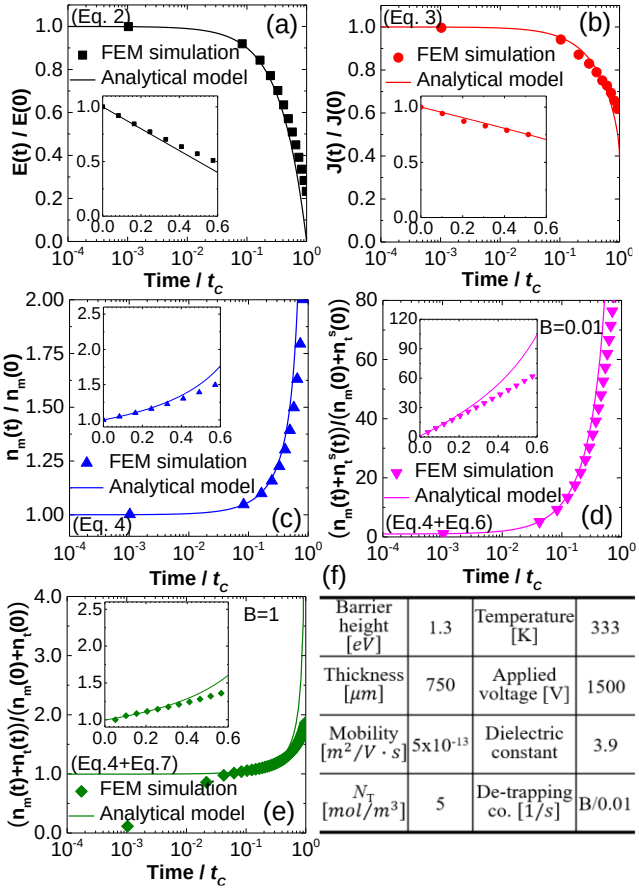

(f)

Barrier height [eV]	1.3	Temperature [K]	333
Thickness [μm]	750	Applied voltage [V]	1500
Mobility [$m^2/V \cdot s$]	5×10^{-13}	Dielectric constant	3.9
N_{T} [mol/m^3]	5	De-trapping co. [$1/s$]	B/0.01

Figure 5. Comparison between the analytical model and FEM simulation: (a) electric field at the electrode, (b) electrons injection flux at the electrode, (c) homocharge concentration at the electrode, (d) homocharge concentration when slow trapping occurs, (e) homocharge concentration when fast trapping occurs, (f) Parameter values for FEM simulation. (insets in Figure 5a~5f) Linear scale on time axis.

mechanisms related to the transport of the injected charges from the opposite electrode: the first involving transport through the water shell layer [2], and the second involving the ultra-fast, soliton-like conduction mechanism explained in [25]. We will demonstrate later in this section these two mechanisms cannot explain the time-evolution of the heterocharge in our devices. In order to study the origin of a heterocharge accumulation, and reduced homocharge injection in wet condition, we can use the analytic model, simulation results and comparison with the experimental data as follows.

The homocharge around an electrode can decrease (Figure 1, top right) *only if* the time derivative of Equation 4 is negative. Equation 9 shows that the condition of $\partial n_{\mathrm{m}}(t)/\partial t < 0$ is satisfied only if

$$\sqrt{E_0\left(1 - \frac{t}{t_{\mathrm{C}}}\right)} < \left[\frac{2kT}{q}\sqrt{\frac{4\pi\varepsilon_{\mathrm{r}}\varepsilon_0}{q}}\right] \tag{9}$$

For $t \ll t_C$ (i.e., ~100s), Equation 9 is satisfied at an unphysically large value of $\varepsilon_{\mathrm{r}} \sim 3.35 \times 10^{12}$ (at T =300 K). Other phenomena, such as pre-existing ions or injected charges from the opposite electrode, must be responsible for the decreasing behavior of homocharge.

Ref. [17] presumed that the origin of heterocharge packet near

anode is due to injected charges (e.g., electrons) from the opposite electrode (i.e., cathode). To assess the hypothesis, we can calculate the effective mobility, $\mu = L/(t \cdot E)$, where L, and t are the distance charge transit and the time it takes to, respectively. Based on the formula, the calculated injected electron μ value is ~ $3.75 \times 10^{-12}(\mathrm{m}^2/\mathrm{V} \cdot \mathrm{s})$ where L, t, and E are 750μm, 10s, and 20kV/mm, respectively. This electron mobility is about an order of magnitude higher compared to that used in the analytical model derivation (see Figure 5f). By Equation 4, we know that high charge mobility would make it impossible to accumulate space-charge concentration observed in PEA experiments. Thus, we can conclude that the injected charge from the opposing contact cannot be the source of the heterocharge accumulation. As an aside, the origin of the ultra-fast heterocharge accumulation is proposed by soliton-like charge pulse [25]. However, its conditions are not satisfied by our experimental condition, namely, much lower electric field (our case, 2MV/m) to form ultra-fast packet (requirement, 5~10MV/m), and much longer time (our case, ~1000s) than the proposed mechanism (typical transit time, ~100ms). Consequently, we conclude that the heterocharge observed in our PEA experiment is due to pre-existing ions (1-20PPM) originated from the fabrication processes and water molecules dissociation (H_3O^+, and OH^-) considering our PEA experiments of the local electric field of 0.2-0.5 V/Å [21].

The analysis above helps us to explain all the space-charge responses shown in Figure 1 and Figure 3.

1. *Reduced homocharge buildup for MC with higher silica filler content:* Increased filler loading increases the effective ε_r because silica fillers have a higher ε_r compared to that of polymer. The amount of homocharge injection can be explained by the ε_r dependent Schottky current expression shown in Equation 2. The characterizations of the ε_r and conductivity of molding compounds equivalent to M73 and M91 are reported in [16]. Indeed, fillers with an even higher ε_r suppress charge injection further [20].
2. *Heterocharge response in dry samples:* Compared to a pure polymer, an EMC must use several additives to improve adhesion between the filler and polymer background. Thus, a EMC has more pre-existing ionic impurities compared to typical polymers, as confirmed by PEA measurement of the initial concentration of ionized impurities. However, since the μ of the pre-existing ions is very low in dry samples, hetero-charge distribution remains almost independent of time, as shown in Figure 1 (left column).
3. *Increased initial homocharge injection in moisture-saturated samples:* The increased amount of initial homocharge injection (compared to the dry samples) can be explained by the increase in the effective ε_r as shown in [17] and the increase of N_T ,and conductivity due to the reaction between water and reaction sites (see Figure 2).
4. *Time dependent reduction of homocharge peak in moisture-saturated samples:* For composites, due to the pre-existing ions from additives and enhanced mobility of pre-existing ions due to water, homocharges are increasingly compensated by the arrival of heterocharges in the vicinity of the electrode, see Figure 1 (top, right).
5. *Increased of heterocharge accumulation in wet samples:* The rapid build-up of heterocharge shown in Figure 1 (bottom, right) can be explained by enhanced transport of the pre-existing ions with the increase in μ and suppression of S with moisture ingress. The larger concentration of pre-existing defects is reflected in the initial concentration determined by the PEA measurement.

6 CONCLUSIONS

Space charge distribution distorts the electric field and reduces the lifetime of various polymer-based encapsulants. Over the years, a number of systems have been analyzed by a variety of analytical techniques and theoretical models, but a comprehensive analysis is lacking. In this paper, we use a broad range of experimental techniques to quantify the space-charge response of commercial-grade epoxy molding compounds and interpreted the results by a simple analytical model for homocharge injection and numerical analysis of the trapping and detrapping dominated heterocharge transport. The model suggests that reliability challenges related to space-charge injection can be reduced by:

1. Suppressing homocharge injection by reducing Schottky injection current, J_0. This can be achieved by increasing the ε_r of the material surrounding the high voltage electrodes, e.g., by using higher ε_r fillers. In addition, reduced polymer defect density N_T through improved processing would also suppress homocharge build-up.
2. Reducing pre-existing ions will suppress heterocharge build-up. Otherwise one must reduce moisture ingress to reduce ion mobility. Interestingly, although heterocharge build-up increases the electric field close to the electrodes, the corresponding charge screening reduces the bulk electric field. If the increased electric field is acceptable, a "dirty" encapsulant may actually reduce the instability of MOSFETs protected by the encapsulants.

To summarize, our numerical approach and the devised compact analytical model can be used to analyze a variety of PEA data obtained for different polymer encapsulants. The insights obtained help to clarify the complicated time dynamics of space charge profiles and suggest new opportunities for the better reliability optimization of an ICs encapsulant.

APPENDIX

Equations for numerical simulation are shown below.

Table A1. Equations for FEM simulation.

Poisson equation: $$-\varepsilon_r\varepsilon_0\frac{\partial}{\partial x}\left(\frac{\partial\varphi(x,t)}{\partial x}\right)=\rho_m(x,t)+\rho_t(x,t)$$	(A1)
$$\rho_m(x,t)=q(p_m-n_m+i_m^+-i_m^-)$$	(A2)
$$\rho_t(x,t)=q(p_t-n_t+i_t^+-i_t^-)$$	(A3)
Continuity equation (n_m, p_m cases are shown, same formula for other ionic species and mobility is zero for trapped species): $$\frac{\partial n_m}{\partial t}+\frac{\partial}{\partial x}\left(\mu_n\cdot n_m\cdot\frac{\partial\varphi(x,t)}{\partial x}\right)=R_{n_m}$$ $$\frac{\partial p_m}{\partial t}-\frac{\partial}{\partial x}\left(\mu_p\cdot p_m\cdot\frac{\partial\varphi(x,t)}{\partial x}\right)=R_{p_m}$$	(A4)
Reaction equation (n_m, n_t cases are shown, same formula for other species, only τ_T and τ_D of ionic species is different): $$R_{n_m}=-R_{n_t}=-\tau_\mathrm{T}\cdot n_\mathrm{m}\cdot\left(1-\frac{n_\mathrm{t}}{N_\mathrm{t}}\right)+\tau_\mathrm{D}\cdot n_\mathrm{t}$$	(A5)

Boundary conditions (GND: $x = 0$, HV:$x = L$): $J_{n_m}(0,t) = J_{p_m}(L,t) = Eq.3$ $J_{n_m}(L,t) = J_{p_m}(0,t) = -\mu_n \cdot n_m \cdot \frac{\partial \varphi(x,t)}{\partial x}$ $i_m^+(0,t) = i_m^+(L,t) = i_m^-(0,t) = i_m^-(L,t) = 0$	(A6)
Initial conditions: $n_m(x,0) = p_m(x,0) = n_t(x,0) = p_t(x,0) = i_m^-(x,0) = i_m^+(x,0) = 0,$ $i_t^-(x,0) = i_t^+(x,0) = 4.2[1/m^3]$	(A7)

Here, p_m, n_m, i_m^+, and i_m^- are mobile holes, mobile electrons, mobile positive ions including pre-existing cations, H_3O^+ from water molecules dissociation, and mobile negative ions including pre-existing anions, OH^- from water molecules dissociation, respectively. Subscription 'm' and 't' in Equation A2 and A3 indicate mobile and trapped, respectively.

Table 2. Input parameters value

Symbol	Meaning	Value
L	Thickness of the sample	750[μm]
T	Temperature	333[K]
ε_r	Dielectric constant	3.9
V	Applied voltage	1500[V]
ϕ_B	Schottky barrier height	1.3[V]
A_0	Richardson constant	1200[$Am^{-2}K^{-2}$]
N_t	Trap density of electrons and holes	50[$1/m^3$]
N_t^i	Trap density of ions	10[$1/m^3$]
μ_n, μ_p	Electron and holes mobility	5×10^{-13}[m^2/V-s]
μ_i^+, μ_i^-	Ions mobility	1.5×10^{-13}[m^2/V-s]
B	Trapping coefficient of electrons and holes	1[s^{-1}]
B_i	Trapping coefficient of ions	0.01[s^{-1}]
S	De-trapping coefficient of electrons and holes	0.001[s^{-1}]
S_i	De-trapping coefficient of ions	0.0002[s^{-1}]

REFERENCES

[1] I. Langmuir, "The effect of space charge and residual gases on thermionic currents in high vacuum," in *Phys. Rev.*, vol. 2, pp. 450-486, Dec. 1913.

[2] D. Fabiani, G.C. Montanari, L. Testa, "Effect of aspect ratio and water contamination on the electric properties of nanostructured insulating materials," in *IEEE Trans. Dielectr. Electr. Insul.*, vol. 17, no. 1, pp. 221-230, Feb. 2010.

[3] S. Palit, D. Varghese, H. Guo, S. Krishnan and M. A. Alam, "The Role of Dielectric Heating and Effects of Ambient Humidity in the Electrical Breakdown of Polymer Dielectrics," in *IEEE Trans. Device Mater. Reliab.*, vol. 15, no. 3, pp. 308-318, Sept. 2015, doi: 10.1109/TDMR.2015.2431998.

[4] X. Jin, C. Jiang, E. Song, H. Fang, J. A. Rogers and M. A. Alam, "Stability of MOSFET-Based Electronic Components in Wearable and Implantable Systems," in *IEEE Trans. Electron Devices*, vol. 64, no. 8, pp. 3443-3451, Aug. 2017, doi: 10.1109/TED.2017.2715837.

[5] A. Aragoneses, I. Tamayo, A. Lebrato, J. C. Canadas, J. Diego, D. Arencon, and J. Belana, "Effect of humidity in charge formation and transport LDPE," in *Journal of Electrostatics*, vol. 71, 04 2013.

[6] G. Mazzanti, G. C. Montanari, and J. M. Alison, "A space-charge based method for the estimation of apparent mobility and trap depth as markers for insulation degradation-theoretical basis and experimental validation," in *IEEE Trans. Dielectr. Electr. Insul*, vol. 10, no. 2, pp. 187-197, Apr. 2003.

[7] T. Fuqiang, Z. Lin, Z. Junliang, and P. Xiao, "Space charge and dielectric behavior of epoxy composite with Sio_2-Al_2O_3 nano-micro fillers at varied temperatures," in *Compos. B. Eng.*, vol. 114, pp. 93-100, 2017.

[8] F. Magraner, A. Garca-Bernab, M. Gil, P. Llovera, S. J. Dodd, and L. A. Dissado, "Space charge measurements on different epoxy resin-alumina nanocomposites," in *2010 10th IEEE International Conference on Solid Dielectrics*, July 2010, pp. 1-4.

[9] Q.Wang and G. Chen, "Effect of nano-fillers on the dielectric properties of epoxy nanocomposites," in *Adv. Mat. Res.*, vol. 1, 03 2012.

[10] N. Liu, M. He, H. Alghamdi, G. Chen, M. Fu, R. Li, and S. Hou, "An improved model to estimate trapping parameters in polymeric materials and its application on normal and aged low-density polyethylenes," in *J. Appl. Phys.*, vol. 118, no. 6, p. 064102, 2015.

[11] M. Praeger, I. L. Hosier, A. F. Holt, A. S. Vaughan, and S. G. Swingler, "On the effect of functionalizer chain length and water content in polyethylene/silica nanocomposites: Part ii charge transport," in *IEEE Trans. Dielectr. Electr. Insul*, vol. 24, no. 4, pp. 2410-2420, 2017.

[12] H. Zhao, C. Xi, X.-D. Zhao and W.-F. Sun, "Elevated-Temperature Space Charge Characteristics and Trapping Mechanism of Cross-Linked Polyethylene Modified by UV-Initiated Grafting MAH," in *Molecules*, vol. 25, no. 17, pp. 397, Aug. 2020.

[13] L. Hui, L. S. Schadler and J. K. Nelson, "The influence of moisture on the electrical properties of crosslinked polyethylene/silica nanocomposites," in *IEEE Trans. Dielectr. Electr. Insul.*, vol. 20, no. 2, pp. 641-653, April 2013, doi: 10.1109/TDEI.2013.6508768.

[14] W. Ahn, D. Cornigli, D. Varghese, L. Nguyen, S. Krishnan, S. Reggiani, M. A. Alam, "Effects of Filler Configuration and Moisture on Dissipation Factor and Critical Electric Field of Epoxy Composites for HV-ICs Encapsulation," in *IEEE Trans. Compon. Packaging Manuf. Technol.*, vol. 10, no. 9, pp. 1534-1541, Sept. 2020, doi: 10.1109/TCPMT.2020.3015658.

[15] I. Imperiale, S. Reggiani, G. Pavarese, E. Gnani, A. Gnudi, G. Baccarani, W. Ahn, M. A. Alam, D. Varghese, A. Hernandez-Luna, L. Nguyen, S. Krishnan, "Role of the Insulating Fillers in the Encapsulation Material on the Lateral Charge Spreading in HV-ICs," in *IEEE Trans. Electron Devices*, vol. 64, no. 3, pp. 1209-1216, March 2017, doi: 10.1109/TED.2016.2645080.

[16] D. Cornigli, S. Reggiani, A. Gnudi, E. Gnani, G. Baccarani, D. Fabiani, D. Varghese, E. Tuncer, S. Krishnan, L. Nguyen., "Characterization of dielectric properties and conductivity in encapsulation materials with high insulating filler contents," in *IEEE Trans. Dielectr. Electr. Insul.*, vol. 25, no. 6, pp. 2421-2428, Dec. 2018, doi: 10.1109/TDEI.2018.007377.

[17] D. Cornigli, S. Reggiani, A. Gnudi, E. Gnani, G. Baccarani, D. Fabiani, D. Varghese, E. Tuncer, S. Krishnan, L. Nguyen, "Electrical characterization of epoxy-based molding compounds for next generation HV ICs in presence of moisture," in Microelectron. Reliab., vol., 88–90, pp. 752-755, Sep. 2018.

[18] J. E. Yagoubi, G. Lubineau, F. Roger, and J. Verdu, "A fully coupled diffusion-reaction scheme for moisture sorption-desorption in an anhydride-cured epoxy resin," in *Polym.*, vol. 53, no. 24, pp. 5582-5595, Nov. 2012.

[19] D. Qiang, Y. Wang, X. Wang, G. Chen, and T. Andritsch, "The effect of filler loading ratios and moisture on DC conductivity and space charge behaviour of SiO_2 and hBN filled epoxy nanocomposites," in *J. Phys. D: Appl. Phys.*, vol. 52., no. 39, pp. 395502, Jul. 2019.

[20] P. Sun, W. Sima, X. Jiang, D. Zhang, J. He and Q. Chen, "Failure of nano-modified oil impregnated paper under repeated impulse voltage: Effects of TiO2 nanoparticles on space charge characteristics," in *IEEE Trans. Dielectr. Electr. Insul.*, vol. 25, no. 6, pp. 2103-2111, Dec. 2018, doi: 10.1109/TDEI.2018.007173.

[21] M. Praeger, I. L. Hosier, A. F. Holt, A. S. Vaughan and S. G. Swingler, "On the effect of functionalizer chain length and water content in polyethylene/silica nanocomposites: Part II — Charge transport," in *IEEE Trans. Dielectr. Electr. Insul.*, vol. 24, no. 4, pp. 2410-2420, 2017, doi: 10.1109/TDEI.2017.005789.

[22] G. C. Montanari, "Bringing an insulation to failure: the role of space charge," in *IEEE Trans. Dielectr. Electr. Insul.*, vol. 18, no. 2, pp. 339-364, April 2011.

[23] G. Lubineau, A. Sulaimani, J. El Yagoubi, M. Mulle, and J. Verdu, "Hysteresis in the relation between moisture uptake and electrical conductivity in neat epoxy," in *Polym. Degrad. Stab.*, vol. 141, pp. 54–57, Jul. 2017.

[24] P. C. Arnett, "Transient conduction in insulators at high fields," in *J. Appl. Phys.*, vol. 46, no. 12, pp. 5236-5243, 1975.

[25] L. A. Dissado, G. C. Montanari, and D. Fabiani, "Fast soliton-like charge pulses in insulating polymers," in *J. Appl. Phys.*, vol. 109, no. 6, p. 064104, 2011.